Received: 2 April 2024 | Revised: 22 May 2024 | Accepted: 2 June 2024

IET Generation, Transmission & Distribution

DOI: 10.1049/gtd2.13202

The Institution of Engineering and Technology WILEY

ORIGINAL RESEARCH

A novel stochastic framework for optimal scheduling of smart cities as an energy hub

Masoud Shokri[1] | Taher Niknam[1] | Mojtaba Mohammadi[1] | Moslem Dehghani[1] | Pierluigi Siano[2,3] | Khmaies Ouahada[3] | Miad Sarvarizade-Kouhpaye[4]

[1]Department of Electrical and Electronics Engineering, Shiraz University of Technology, Shiraz, Iran

[2]Department of Management and Innovation Systems, University of Salerno via Giovanni Paolo II, Fisciano, Italy

[3]Department of Electrical and Electronic Engineering Science, University of Johannesburg, Johannesburg, South Africa

[4]Instituto de Investigación Tecnológica, Comillas Pontifical University ICAI School of Engineering, Madrid, Spain

Correspondence
Taher Niknam, Department of Electrical and Electronics Engineering, Shiraz University of Technology, Shiraz, Iran.
Email: niknam@sutech.ac.ir

Abstract

Smart cities consist of various energy systems and services that must be optimally scheduled to improve energy efficiency and reduce operation costs. The smart city layout comprises a power distribution system, a thermal energy system, a water system, and the private and public transportation systems. Additionally, several new technologies such as reconfiguration, regenerative braking energy of the metro, etc. are considered. This study is one of the first to consider all these technologies together in a smart city. The proposed power distribution system is a grid-connected hybrid AC–DC microgrid. The biogeography-based optimization algorithm was utilized to seek the best solution for scheduling micro-turbines, fuel cells, heat pumps, desalination units, energy storage systems, AC–DC converters, purchasing power from the upstream, distributed energy resources, and transferring power amongst electric vehicle parking stations and metro for the next day. Also, the reduced unscented transformation layout was used to capture the system's uncertainty. The suggested layout is implemented on an enhanced IEEE 33-bus test system to show the efficiency of the suggested method. The results show that costs and environmental pollution are reduced. By comparing the proposed smart city with other studies, the efficiency and completeness of the proposed smart city are shown.

1 | INTRODUCTION

The world's population that have been living in urban regions is growing. It is estimated that in 2050, nearly 68 percent of the world's population will live in urban regions [1]. Therefore, more challenges will arise due to limited services and resources, including energy and transportation [2].

The smart cities (SCs) idea has been created and improved along with the integration of information and communication technology (ICT) in urban environments [2, 3]. The SC is considered to be a solution to urban issues. It enhances the social and economic aspects of the lives of the residents through sustainable services and systems [1–3]. The power system, the thermal energy system, the water system, the private transportation system, and the public transportation system are considered as the systems that are operated with their interconnection through the SC. These systems consist of several types of energy resources like wind turbines (WTs), photovoltaic (PV) panels, micro-turbines (MTs), fuel cells (FCs), heat pumps (HPs), desalination units (DUs), energy storage systems (ESSs), bi-directional AC–DC converter, electric vehicles (EVs), and the metro system. To improve energy efficiency and reduce the operation costs in the SC, these technologies should be optimally scheduled a day ahead. It should be noted that there are some sources of uncertainties, for example, the energy price, which should be taken into account to achieve a reliable and effective energy management (EM) scheme. Hence, a day-ahead stochastic optimization framework (SOF) should be designed to reach a cost-effective operation. However, the diversity of technologies, the interconnection between the systems, uncertainties, and the operational constraints impose significant challenges on EM of SCs. Therefore, proposing an applicable and comprehensive optimization framework to optimally schedule the operation of a SC would be of interest.

Many researches have focused on SC modelling, optimum operation, and EM of SCs. In [4], a deep learning layout has been utilized to forecast the short-term energy consumption (EC) of a SC. Then the forecasting results are used to optimally schedule the operation of the SC. In [5], a cyber-secure stochastic EM scheme for the SCs is proposed applying the intelligent priority selection method. It is considered that a SC includes the microgrid (MG), the EVs, and the metro system. A coordinated optimal scheduling scheme has been considered in [6] to minimize the EC costs of the metro systems, considering the interrelation between the power network, ESSs, and the railway network. Researchers in [6] assume that the rail transit trains are controllable loads/sources in tractive/brake mode. Hence, the demand response scheme could be employed to reduce the EC costs while maintaining driving comfort. In [7], a SOF is presented to optimize the operation of a SC that investigates the cooperation of the buildings, the EVs, and the metro system based on the point estimate scheme. To reduce the operation cost, it is assumed that the regenerative braking energy of the metro and stored energy on EVs can be used to supply electrical demands through vehicle-to-subway (V2S) and vehicle-to-grid (V2G) applications. An EM framework is presented in [8] to optimize the operation of a SC considering V2S and V2G technologies. Furthermore, the unscented transformation (UT) layout was used to take the uncertainties of the transportation systems and production of WTs in a correlated environment. In [9], a flexible power-water scheme has been suggested to optimize the scheduling of the interdependent power and water distribution systems. The obtained simulation results highlight the energy flexibility that is provided by the DUs. In [10], a SOF is proposed for SC water management. In this regard, the particle swarm optimization (PSO) algorithm is considered to optimally schedule the controllable water pumping units. In [11], an optimal scheduling model is proposed for the district cooling system of large buildings in SCs considering cooling load uncertainties. A robust chance-constrained approach is employed in [12] to optimize the operation of the multi-zone heating, ventilation, and air-conditioning (HVAC) system in SCs.

Although the mentioned research papers considered the important aspects of the optimal operation of SCs, none of the published works propose a comprehensive optimization framework that considers the interconnection between the power system, the thermal energy system, the water system, and the private and public transportation systems in a SC. Moreover, the optimal reconfiguration of distribution power systems is not addressed in research on the optimal operation of SCs. Some works such as [13–16] show that the optimal reconfiguration can lead to a significant operating cost reduction due to reducing power losses. In [17], a model for co-optimization operation and planning of smart transportation systems in a SC, considering the thermal system, is provided. The UT method has been applied to take the uncertainties of the suggested scheme. However, the presented SC model does not consider the water system and network reconfiguration is not performed. The synergies between smart transportation systems and thermal system within a SC is investigated in [18]. Similarly, the water system and network reconfiguration are missing from this research. In [19], the optimum operation of the distribution feeder reconfiguration scheme in a smart grid with a high influence of EVs and WTs is proposed. This research lacks smart urban transportation modelling along with thermal and water systems modelling. In [20] similarly to this paper, an EM and scheduling framework is proposed for MGs. However, it lacks smart transportation, thermal system, water system, and network reconfiguration modelling. The advantages and disadvantages of the previously mentioned papers have been illustrated in Table 1.

It is noteworthy that finding an optimum EM layout for the mentioned SC is challengeable due to the high interconnectivity amongst systems through modern technologies. In addition, the existing uncertainties further increase the difficulties.

In this study, a SOF has been considered to optimize the operation of a SC. The SC is comprised of a power distribution system, a thermal energy system, a water system, a private transportation system, and a public transportation system which includes the connection between the electric vehicle and the subway system by a battery in the subway station, where the energy from the regenerative braking of the subway is stored in the battery. This energy can be used between the EVs and the subway. As well as this is the first study considering all these technologies in a SC. The power distribution system is a grid-connected hybrid AC–DC MG equipped with a bi-directional AC–DC converter. It has been presumed that the regenerative braking energy of the metro and stored energy on EVs can be used to supply electrical demands through the V2G and V2S applications. The proposed optimization method is designed to schedule the MTs, the FCs, the HPs, the DUs, the ESSs, the bi-directional AC–DC converters, the purchasing power from the upstream network and the distributed energy resources (DERs), as well as the transferring power among the EV parking stations and the metro for the next day. Also, a HP system for providing thermal energy that has a high efficiency has been considered to provide thermal energy by the gas system purchased from the network. In this problem, a sea water purification system is assumed due to the possible limitation in future water consumption. The reduced unscented transformation (RUT) scheme is utilized to capture the uncertainty of the energy price. The biogeography-based optimization (BBO) algorithm is utilized to solve the optimization problem (OP).

The suggested scheme is implemented on an enhanced IEEE 33-bus trial network. The major contributions of the paper are explained in the following:

- Proposing a comprehensive optimization scheme to optimally schedule a SC.
- Considering various energy carriers including the electrical, water, thermal, and transportation as well as different technologies such as reconfiguration, regenerative braking energy of the metro, etc. in SCs simultaneously.
- Addressing the network reconfiguration in the optimal EM scheme of the SC.

TABLE 1 Advantages and disadvantages of the references.

Reference	Smart transportation	Uncertainty modelling	Network reconfiguration	Thermal system	Water system
[5]	✓	✓	✗	✓	✗
[7]	✓	✓	✗	✗	✗
[8]	✓	✓	✗	✗	✗
[17]	✓	✓	✗	✓	✗
[18]	✓	✓	✗	✓	✗
[19]	✗	✓	✓	✗	✗
[20]	✗	✓	✗	✗	✗
Our study	✓	✓	✓	✓	✓

- Applying the RUT method to capture uncertainties and utilizing the BBO algorithm to solve the proposed stochastic OP.

The remaining sections of paper have been organized as follows: Section 2 illustrates the mathematical formulation of the OP for the optimum scheduling of the SC. Section 3 describes the SOF for optimal scheduling of the SC. The case study descriptions and simulation outcomes have been explained in Section 4. Eventually, the conclusions and possible future works have been illustrated in Section 5.

2 | PROPOSED OPTIMIZATION PROBLEM FOR OPTIMAL SCHEDULING

An OP has been formulated in this section to optimize the SC's operation. The system operator can schedule existing DERs and purchase/sell energy from/to the upstream grid the next day using the proposed method. Various types of electrical loads such as residential loads, air-source HPs, DUs, and electrical transport systems are connected to buses of the system. The electrical, heat, and water demand (WD) can be supplied by the upstream network and DERs such as PV panels, WTs, ESSs, FCs, MTs, HPs, DUs, EV parking stations, and public transport systems. In the case of public transport systems, especially the metro, the regenerative braking energy can circle back to the grid to directly serve customers or be stored in EV batteries or ESSs.

2.1 | Objective function (OF)

The OF of the proposed OP has been illustrated in Equation (1), where DER shows the set of DERs including PV panels, WTs, ESSs, FCs, MTs, HPs, DUs, EV parking stations, and the metro. Equation (1) is comprised of five parts. The first part presents the energy cost of the DERs. The second, third, and fourth parts show the energy cost of the electrical, thermal, and water networks bought from the upstream grids or the corresponding DERs, respectively. The fifth part is the degradation cost (DgC) of EV batteries. The first part consists of the energy purchase cost from the DERs, the DERs' startup and shutdown costs. In Equation (1), it is noteworthy that the power of ESSs, EV parking, and the metro have a negative sign which are injected into the upstream grid and the parameters; otherwise, it has a positive sign. The proposed OP has been solved to minimize the SC's operation. The OP has been subjected to several operational constraints which are introduced in the following.

$$\min F = \sum_{i\in DER}\sum_{j=1}^{N_i}\sum_{t=1}^{T}\left(\begin{matrix}u_{i,j,t}\,P_{i,j,t}\,\lambda_{i,j,t}+\lambda_{i,j}^{ON}\max(0,u_{i,j,t}\\-u_{i,j,t-1})+\lambda_{i,j}^{OFF}\max(0,u_{i,j,t-1}-u_{i,j,t})\end{matrix}\right)$$
$$+\sum_{t=1}^{T}P_t^G\lambda_t^G+\sum_{t=1}^{T}P_t^{Thermal}\lambda_t^{Heat}+\sum_{t=1}^{T}W_t^G\lambda_t^{Water}+\lambda_{\deg}^{EV} \quad (1)$$

2.2 | Power balance constraints

The constraints of power balance should be met in both the AC and DC subgrids. Equation (2) presents the power balance equation in AC sub-grid. In Equation (2), $P_t^{loss,AC}$ that represents the power losses in AC sub-grid. Equations (4) and (5) represent the system's active and reactive power flow, respectively. The power balance equation in DC sub-grid is displayed in Equation (6).

$$\sum_{i\in DER^{AC}}\sum_{j=1}^{N_i^{AC}}P_{i,j,t}+P_t^G=\sum_{k=1}^{K^{AC}}P_{k,t}^L+P_t^{loss,AC}\qquad\forall t \quad (2)$$

$$P_t^{loss,AC}=\sum_{i=1}^{N_{branch}}R_i\times\left|I_{i,t}\right|^2 \quad (3)$$

$$P_t^{inj,AC}=\sum_{k=1}^{K^{AC}}\sum_{k'=1}^{K^{AC}}V_{k,t}V_{k',t}Y_{k,k'}\cos(\theta_{k,k'}+\delta_{k,t}-\delta_{k',t})\qquad\forall t \quad (4)$$

$$Q_t^{inj,AC}=\sum_{k=1}^{K^{AC}}\sum_{k'=1}^{K^{AC}}V_{k,t}V_{k',t}Y_{k,k'}\sin(\theta_{k,k'}+\delta_{k,t}-\delta_{k',t})\qquad\forall t \quad (5)$$

$$\sum_{i\in DER^{DC}}\sum_{j=1}^{N_i^{DC}}P_{i,j,t}+P_t^C=\sum_{k=1}^{K^{DC}}P_{k,t}^L+P_t^{loss,DC}\qquad\forall t \quad (6)$$

Equations (2)–(6) indicate that the sum of electrical generations should be equalized to the total electrical loads and power losses in each sub-grid.

2.3 | Capacity constraints

Equation (7) limits the power which is purchased/sold from/to the upstream grid in each time step. The power of the DERs is limited by Equation (8). Additionally, Equation (9) limits the power which is transferred by the bi-directional converter.

$$P^{G,\min} \le P_t^G \le P^{G,\max} \qquad \forall t \tag{7}$$

$$P^{\min} \le P_{i,j,t} \le P^{\max} \qquad \forall i,j,t \tag{8}$$

$$P^{C,\min} \le P_t^C \le P^{C,\max} \qquad \forall t \tag{9}$$

2.4 | Line capacity constraint

The amount of power flow that is allowed through the lines is specified by Equation (10).

$$\left|P_{k,k'}^{Line}\right| \le P_{k,k'}^{Line,\max} \qquad \forall k,k' \tag{10}$$

2.5 | Voltage magnitude constraint

The allowable range for the voltage of buses is determined by Equation (11.)

$$V_{k,t} \le V^{\max} \quad \forall k,t \tag{11}$$

2.6 | Ramp rate constraint

Equation (12) limits the increment or decrement in the power of the DERs.

$$\left|P_{i,j,t} - P_{i,j,t-1}\right| \le RR_{i,j} \quad \forall i,j,t \tag{12}$$

2.7 | EES constraints

The state of charge (SOC) of the jth EES could be calculated using Equation (13). It is noted that when the system operator receives the power from an ESS, the power has a positive sign; otherwise, it has a negative sign. The allowable range of SOC for an ESS is determined by Equation (14). Equation (15) guarantees that the charging and discharging cannot occur at the same time.

$$S_{j,t}^{EES} = S_{j,t-1}^{EES} - \left(B_{j,t}^{C,ESS} P_{i,j,t}\, \eta^{C,ESS} + B_{j,t}^{D,ESS} P_{i,j,t} / \eta^{D,ESS}\right)\Delta t$$
$$i \in \{EES\} \qquad \forall j,t \tag{13}$$

$$S^{EES,\min} \le S_{j,t}^{EES} \le S^{EES,\max} \qquad \forall j,t \tag{14}$$

$$B_{j,t}^{C,ESS} + B_{j,t}^{D,ESS} \le 1 \qquad \forall j,t \tag{15}$$

2.8 | EV parking constraints

The summation of stored energy in EVs that are parked in the jth EV parking lot can be calculated by Equation (16). Equation (16) is comprised of five terms. The first term shows the amount of stored energy in the available EVs in the parking lot at the previous time step. The second term, indicated by 1, represents the interaction between the EV parking and the grid. The third term indicates the summation of the initial SOC of EVs that are connected to the EV parking at the present step. The fourth term is the summation of SOC of EVs that are disconnected from the EV parking at the present step. The fifth term, indicated by 2, shows the interaction among the EV parking and the metro. It is noted that when the system operator receives the power from an EV parking, the power has a positive sign; otherwise, it has a negative sign.

$$S_{j,t}^{EV} = S_{j,t-1}^{EV} - \underbrace{\left(B_{j,t}^{C,EV} P_{i,j,t}\, \eta^{C,EV} + B_{j,t}^{D,EV} P_{i,j,t} \Big/ \eta^{D,EV}\right)\Delta t}_{1}$$
$$+ S_{j,t}^{EV,Arr} - S_{j,t}^{EV,Dep}$$
$$+ \underbrace{\left(P_{j,t}^{Metro-EV}\, \eta^{C,EV} - P_{j,t}^{EV-Metro} \Big/ \eta^{D,EV}\right)\Delta t}_{2}$$
$$i \in \{EV\} \quad \forall j,t \tag{16}$$

The allowable range for the SOC of the jth EV parking lot is determined by Equations (17) and (18). The allowable power exchange between an EV parking and the metro is limited by Equations (19) and (20). Equation (21) ensures that the power exchange between EV parking and the metro is not happening in both directions at the same time.

$$S_{j,t}^{EV} \le S^{Ind,\min} N_{j,t}^{EV} \qquad \forall j,t \tag{17}$$

$$S_{j,t}^{EV} \ge \sum_{v=1}^{N_{j,t}^{EV}} BC_v \qquad \forall j,t \tag{18}$$

$$0 \le P_{j,t}^{Metro-EV} \le P^{Metro-EV,\max} B_{j,t}^{Metro-EV} \qquad \forall j,t \tag{19}$$

$$0 \le P_{j,t}^{EV-Metro} \le P^{EV-Metro,\max} B_{j,t}^{EV-Metro} \qquad \forall j,t \tag{20}$$

$$B_{j,t}^{EV-Metro} + B_{j,t}^{Metro-EV} \le 1 \qquad \forall j,t \tag{21}$$

2.9 | Metro constraints

This paper assumes that the regenerative energy of the metro can be used to charge EVs in a parking lot or to supply trains. It is noteworthy that the transferred power from the metro to an EV parking is limited by $P^{Metro-EV,max}$, which depends on the available regenerative energy. In addition, the power can be transferred from an EV parking to the metro. With this in mind, the transmitted power from the grid to the metro can be

calculated by Equation (22)

$$P_{i,j,t} = P_{j,t}^{MetroAct} - P_{j,t}^{Bra} - P_{j,t}^{EV-Metro} \quad i \in \{Metro\} \quad \forall j,t \tag{22}$$

2.10 | Heat balance constraint

The heat demand can be supplied by HPs and the thermal energy system. Hence, the heat balance constraint has been displayed as Equation (23).

$$P_t^{Thermal} = \sum_{h=1}^{H} P_{h,t}^{Heat} - \sum_{i} \sum_{j=1}^{N_i} P_{i,j,t} \quad i \in \{HP\} \quad \forall t \tag{23}$$

2.11 | Water system constraints

The WD supplement system is comprised of a DU, an initial tank, and a freshwater tank (FWT). The DU is supplied by sea water and electricity. Then the desalinated water has been transferred to the secondary tank. The FWT has been linked to the primary tank as well as the water grid. The WDs, for example, the WD of the metro and buildings, are supplied by the FWT. In the following equations, the water system model is formulated. The stored water amount in the primary tank can be calculated by Equation (24). The FWT water volume at the time step t is presented by Equation (25). The allowable range of the stored water in the primary tank and the FWT are determined by Equations (26) and (27), respectively. Finally, the consumed power of the DU can be calculated by Equation (28).

$$U_t^{PT} = U_{t-1}^{PT} + W_t^{DU,in} - W_t^{DU,out} \quad \forall t \tag{24}$$

$$U_t^{FWT} = U_{t-1}^{FWT} + W_t^{DU,out} + W_t^{G} - W_t^{demand} \quad \forall t \tag{25}$$

$$0 \le U_t^{PT} \le U^{PT,\max} \quad \forall t \tag{26}$$

$$U^{FWT,\min} \le U_t^{FWT} \le U^{FWT,\max} \quad \forall t \tag{27}$$

$$P_{i,j,t} = W_t^{DU,in} CF^{DU} \quad i \in \{DU\} \quad \forall t \tag{28}$$

2.12 | Degradation cost of EV batteries

The battery degradation happens due to the battery's charging/discharging cycles. The depth of discharge *(DoD)* obtained by the Wöhler curve, indicates the number of cycles which the battery is able to be charged and discharged [19]. A typical Wöhler curve of a battery has been displayed in Figure 1. Equation (29) defines the Wöhler curve formulation, in which a and b defines the constants relevant to the battery type and n_{Cycle} *(DoD)* shows the number of possible cycles according to the DoD value [19]. For produced Li-ion batteries in Saft company, the variables $a = 1331$ and $b = -1.825$ have been acquired [21].

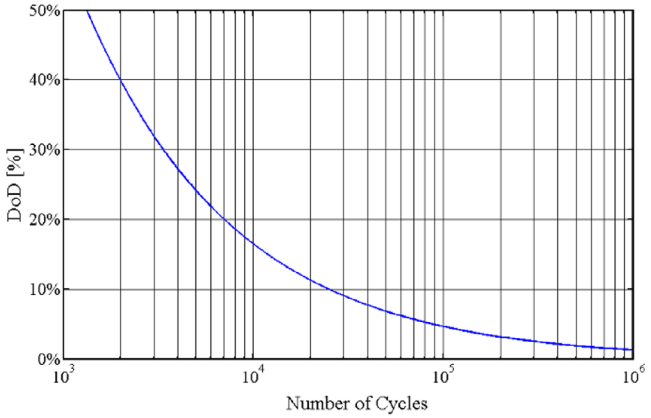

FIGURE 1 The lithium-ion battery's Wöhler curve.

The DgC of discharging the battery from the fully charged mood, that is, DoD equals to zero, to a determined charge level, that DoD equals to DoD_{spec}, which has been computed in Equation (30), in which E^{EVBat} defines the usable energy of the battery (kWh).

$$n_{cycle}(DoD) = a.DoD^{b} \tag{29}$$

$$\lambda_{\deg}(0, DoD_{spec}) = \frac{\lambda_{ins}^{EVBat} * DoD_{spec} * E^{EVBat}}{n_{cycle}(DoD_{spec})} \tag{30}$$

The discharge cycle's DgC from $DoD_{initial}$ to DoD_{final} is computed via Equation (31). Eventually, in Equation (32), the total DgC has been presented which is the whole DgCs over the number of discharges.

$$\lambda_{\deg}(DoD_{initial}, DoD_{final}) = \lambda_{\deg}(0, DoD_{final}) - \lambda_{\deg}(0, DoD_{initial}) \tag{31}$$

$$\lambda_{\deg}^{EV} = \sum_{n_{dis}} \lambda_{\deg,n}(DoD_{initial}, DoD_{final}) \tag{32}$$

3 | SOF FOR OPTIMAL SCHEDULING OF THE SMART HYBRID MG

In this section, a SOF is presented to solve the proposed OP considering uncertainties. Due to the high volume of calculations caused by the complete smart city system, there is a need for powerful and fast methods to deal with uncertainty and problem solving. Using the RUT method, the speed of solving problems with uncertainty has increased (the speed of solving problems has doubled). Hence, RUT technique has been used to model the uncertainty regarding to the market price. In addition, the BBO algorithm has been utilized to seek the best solution in the proposed OP.

3.1 | Reduced unscented transformation

Three main methods exist for uncertainty modeling, including the Monte Carlo simulation (MCS), analytical techniques, and approximate techniques [22]. The MCS is a well-known method to investigate the uncertain behavior of random variables in a problem. To reach this goal, numerous scenarios are generated and the problem is solved according to each generated scenario. Then the statistical characteristics of decision variables (for example the mean value) and the OF can be calculated. Although the MCS can reach accurate results, it requires a high computational cost. Hence, it is not recommended for short-term scheduling tasks. In contrast, analytical techniques are computationally more efficient but simplify the problem with some mathematical assumptions [23]. Approximate methods, namely the unscented transformation method, have overcome these shortcomings.

For the nonlinear problem $y = f(x)$, X is the random input whose length is equal to the number of unknown parameters. Additionally, f and y define the nonlinear function and the output vector, respectively. In addition, μ represents the mean value and P_{xx} is the covariance. Like the two-point estimation method, the problem is solved $2m + 1$ times to model uncertainties in the UT. In contrast, the problem is solved $m + 2$ times in the RUT. Hence, the RUT technique is faster than the UT method. As a result, complex stochastic OPs can be solved faster and easier. In the following, a step-by-step description of the RUT scheme has been presented to model the uncertainties [24].

Step 1. Selecting the free parameter W_0 within [0, 1] range;
Step 2. Selecting the weight sequence using: $W_i = \frac{1-W_0}{m+1}$
Step 3. Initializing the vector sequence using:

$$x_0^1 = [0], x_1^1 = \begin{bmatrix} -1 \\ \sqrt{2W_1} \end{bmatrix}, x_2^1 = \begin{bmatrix} 1 \\ \sqrt{2W_1} \end{bmatrix} \quad (33)$$

Step 4. Expanding vector sequence on j set using:

$$x_i^j = \begin{cases} \begin{bmatrix} x_0^{j-1} \\ 0 \end{bmatrix}, & \\ \begin{bmatrix} x_i^{j-1} \\ \frac{-1}{\sqrt{j(j+1)W_1}} \end{bmatrix}, & i = 1, \ldots, j \\ \begin{bmatrix} 0_{j-1} \\ \frac{j}{\sqrt{j(j+1)W_1}} \end{bmatrix}, & i = j+1 \end{cases} \quad (34)$$

Step 5. Giving $m + 2$ input sigma points to the nonlinear function and getting the output samples using: $Y^i = f(x^j)$;
Step 6. Calculating the mean and covariance matrix of the output Y using: $\mu_j = \sum_{i=0}^{P} W_i y_i$ and $P_{yy} = \sum_{i=0}^{P} W_i (y_i - \mu_i)(y_i - \mu_i)^T$.

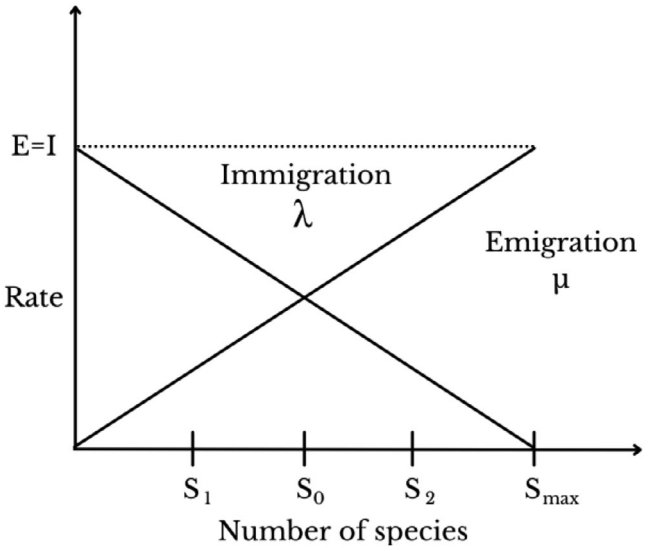

FIGURE 2 Emigration, and immigration rate model.

3.2 | BBO algorithm

The BBO algorithm is a population-based evolutionary algorithm which utilizes migration and mutation concepts to probabilistically adapt the solutions [25]. BBO algorithm has distinctive characteristics that separate it from other algorithms which are explained briefly in the following [26]. In BBO, similar to PSO, solutions are not eliminated at the end of each generation unlike the genetic algorithm (GA), and differential evolution (DE). Additionally, in the evolutionary optimization algorithms, lots of solutions with good fitness values lose their quality due to crossover operation, while in BBO solutions get better through the migration process. However, PSO solutions gave a greater chance of sticking together in similar clusters, unlike BBO where the solutions do not cluster together because of the mutation process. Another unique characteristic of the BBO algorithm is that bad solutions get features from better solutions to improve. This feature makes constraint satisfaction easier than that in the bacterial foraging algorithm (BFA) [26].

The mathematical model of BBO represents the way species immigrate and emigrate between different habitats. The habitats that are suitable for species have been considered to have higher habitat suitability index (HSI) [27]. Additionally, the parameters that characterize habitability are named the suitability index variables (SIVs) [25]. Most of the species have resided in habitats with high HSI. Accordingly, the habitats' immigration rate is low and the habitats' emigration rate is high, due to their large population. Conversely, habitats with low HSI, include a small number of species. Moreover, habitats with low HSI consist of a high immigration ratio and low emigration ratio due to their small population. Low HSI habitats may improve due to the immigration of new species. Also, the species may go extinct if the HSI remains low.

A habitat defines a probable solution of the OP, while HSI is represented the fitness of every solution. A model of species abundance has been displayed in Figure 2, that λ and μ define

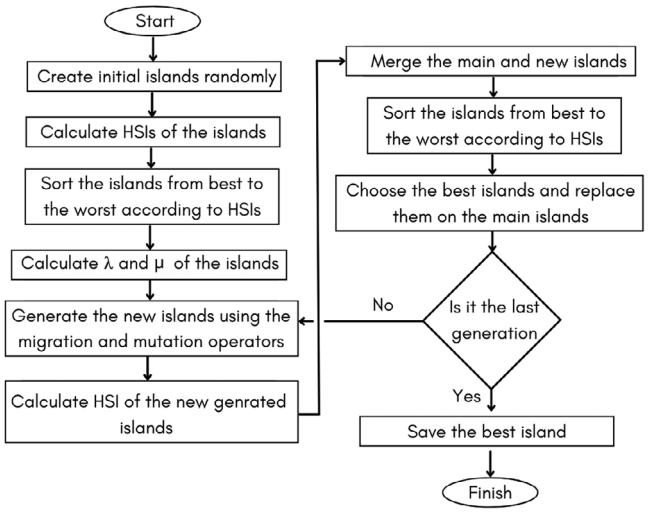

FIGURE 3 Flowchart diagram of the BBO algorithm.

the immigration and emigration rates, respectively, and also S defines the number of species. It should be noted that I and E define the maximum possible immigration and emigration rates, respectively. For the sake of brevity, it is assumed that the emigration and immigration habitats represent the linear functions of habitats HSI and E and I are equal. Also, these rates depend on the number of species in the habitats.

For each solution H_i, the immigration and emigration ratios have been calculated using Equations (35) and (36), where k_i represents the number of species, and n is the maximum number of species.

$$\mu = E\left(\frac{k_i}{n}\right) \tag{35}$$

$$\lambda = I\left(1 - \frac{k_i}{n}\right) \tag{36}$$

The mathematical model for the immigration and emigration processes is illustrated via the probabilistic layout. P_s represents the probability where S species are in the habitat at time t. Equation (37) shows this probability between t to $t + \Delta t$, that μ_s and λ_s are emigration and immigration rates at the time. Also, S species are in the habitat. Equation (38) is the limitation of Equation (37) as Δt approaches zero.

$$P_s(t + \Delta t) = P_s(t)\,(1 - \lambda_s \Delta t - \mu_s \Delta t) + P_{s-1}\lambda_{s-1}\Delta t + P_{s+1}\mu_{s+1}\Delta t \tag{37}$$

$$P_s = \begin{cases} -(\lambda_s + \mu_s)\,P_s + \mu_{s+1}P_{s+1} & S = 0 \\ -(\lambda_s + \mu_s)\,P_s + \lambda_{s-1}P_{s-1} + \mu_{s+1}P_{s+1} & 1 \le S \le S_{max} \\ -(\lambda_s + \mu_s)\,P_s + \lambda_{s-1}P_{s-1} & S = S_{max} \end{cases} \tag{38}$$

A step-by-step guide to the execution of the BBO algorithm has been illustrated [28]. In addition, the flowchart of the suggested algorithm is depicted in Figure 3.

Step 1: Adjust input amounts consist of the number of variables, maximum iteration, and number of the population. In which, the N defines the population number and it is assumed to equal 400. The maximum number of iteration is assumed as 700, and m_i defines the number of species in habitat i. Initialize BBO parameters including maximum immigration ratio, maximum emigration ratio, mutation probability $P_{mutation}$, and the habitat modification probability P_{mod}. The keep-rate is equal to 0.2 meaning that 20 percent of the best habitats are kept with no change and 80 percent of the habitats are changed. Finally, set $\alpha = 0.9$, and $\delta = 0.02 \times (X_{max} - X_{min})$ as the hyperparameters of the algorithm.

Step 2: Generating the initial population by random. Further, the primary population should convince the constraints. To guarantee this, X_{max} and X_{min} have been computed based on the maximum and minimum variables' limits. Next, the primary population has been computed applying Equation (39). In which *rand* defines a random vector amongst zero to one.

$$\bar{X}_{pop} = (rand * (X_{\max} - X_{\min})) + X_{\min} \tag{39}$$

This procedure has been repeated for each parameter, for the population number, so that the primary population has been computed.

Step 3: Releasing the whole constraints of the problem via applying the following equation:

$$G(X) = [f(\bar{X})] + L_1\left(\sum_{1}^{N_{\text{eq}}} (h_{\text{eq}}(\bar{X}))^2\right) + L_2\left(\sum_{1}^{N_{\text{ineq}}} (Max[0, -g_{\text{ineq}}(\bar{X})])^2\right) \tag{40}$$

In which $f(\bar{X})$ defines the OF of the problem. $g_{ineg}(\bar{X})$ and $h_{eq}(\bar{X})$ express the inequality and equality restrictions, respectively. Two variable that is affected the efficiency of the method are L_1 and L_2 penalty values. If the penalty values are chosen too high, the method could be trapped in the local minima. Also, if the penalty values are chosen too low, they cannot find the feasible optimal solutions. An adaptive penalty function applying in [29] has been extracted to determine the penalty variables. For brevity, $\sum_1^{N_{eq}} (h_{eq}(\bar{X}))^2$ and $\sum_1^{N_{ineq}} (Max[0, g_{ineq}(\bar{X})])^2$ have been defined as B and $L_1 = L_2 = i\sqrt{i}\lambda\beta^{\delta}$. In which, i defines the iteration number, δ presents the power of the penalty value, and λ is a multi-step assignment value. if $B \le 1$ then $\delta = 1$, otherwise $\delta = 2$. In addition, if $B \le 0.001$, then $\lambda = 1$, else if $B \le 0.01$, then $\lambda = 10$, else if $B \le 0.1$, then $\lambda = 30$, otherwise $\lambda = 100$.

Step 4: Compute the OF with the population for given immigration and emigration rates. Ordering the

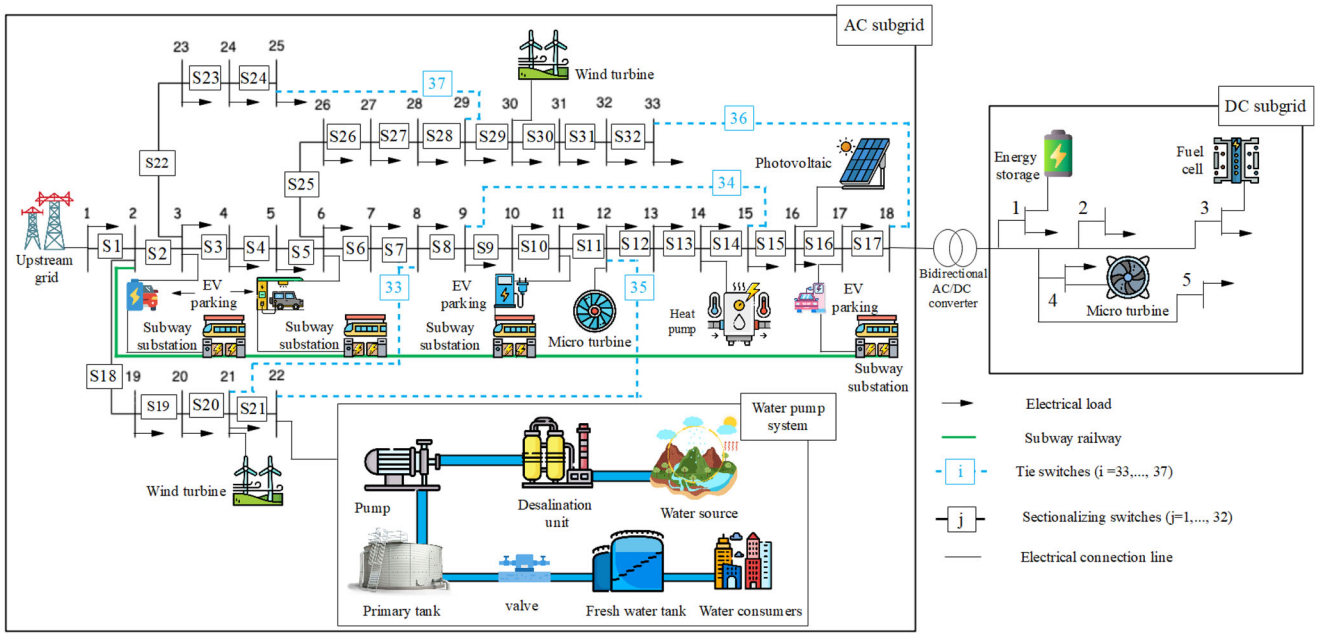

FIGURE 4 The test system [20].

population on the basis of the OF values. Then set the sorted population as $\bar{X}_{pop-sorted}$ and best answer as X_{best}.

Step 5: Performing the probabilistic migration on SIVs of the 80 percent lower population of the $\bar{X}_{pop-sorted}$. Apply the roulette wheel selection according to the emigration rates to choose emigrating islands. First, the emigration and immigration rates for each habitat set must be calculated. Next, the habitats and SIVs are chosen for newly produced habitats after migration.

Step 6: Performing probabilistically mutation according to $P_{mutation}$ for entire habitats.

Step 7: Calculate the OF for every mutated habitat.

Step 8: Update X_{pop} and go to step 4 until the iteration number reaches to maximum.

4 | NUMERICAL RESULTS

The efficiency and applicability of the suggested scheme are demonstrated in this part. The offered scheme has been performed on an improved test system presented in [20]. The considered system in [20] is a modified IEEE 33-bus trail network. The heat, water, and public transport systems as well as the EV parking lots and manoeuvre switches are added to that system to represent a more complete SC model in this paper. Figure 4 depicts the proposed test system.

4.1 | Assumptions and parameters

The test system includes one HP, one ESS, two MTs, one FC, four EV parking stations, and one metro railway that includes four electrical substations, one DU, one AC–DC converter, and five manoeuvre switches. The specifications of the MTs, the FC, the ESS, and the converter as well as the electrical system data and the market price are the same as the assumed values in [20]. The AC and DC sub-grids have 12.6 and 1.0 kV voltage levels, respectively. It should be noted that renewable energy resources, that is, PV panels and WTs, have been investigated as non-dispatchable units. For simplicity, the resistance of the line in the DC sub-grid has not been considered. The data of the EV parking stations, the metro, the HP, and the thermal system are taken from [30]. Also, almost 95% of the thermal energy is supplied by

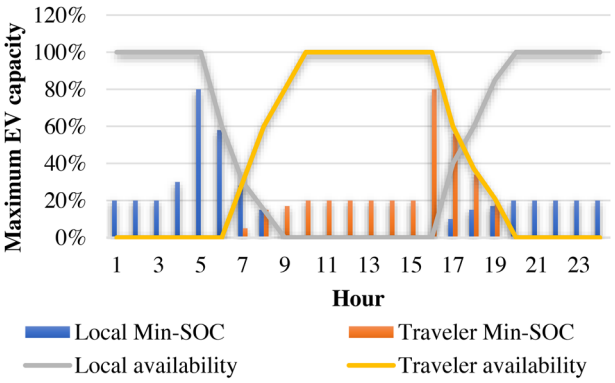

FIGURE 5 EV users' TOU and minimum SOC requirements.

TABLE 2 Simulation case studies.

No. of cases	Technologies (e.g., HP, EES, MT, FC, etc.)	Regenerative braking energy	Network reconfiguration
Case I	✓	✓	✓
Case II	✓	✓	✗
Case III	✓	✗	✓

TABLE 3 Specification of the trial system.

Kind	Min-power (kW)	Max-power (kW)	Bid ($/kWh)	Startup/ startdown ($)	Location
MT_2	0	2000	0.675	75	12
WT_1	0	250	1.073	0	30
WT_2	0	550	1.073	0	21
PV	0	400	2.584	0	16
HP	0	400	Market-price	0	14
FC	0	700	0.394	38.5	DC-MG
MT_1	0	350	0.48	68	DC-MG
Energy storage	−350	350	0.318	0	DC-MG
AC/DC Converter	−1500	1500	0	0	DC-MG

the HP unit. Here, two diverse types of EV users such as local users and traveler users have been investigated. The parking lots of local users have been used at night when they come back to their houses, while the traveler users are used the parking within the day when the local users are gone. To increase the battery life, it is presumed that the maximum and minimum SOC of the parked EVs are 80% and 20%, respectively, when the EVs leave [31]. As well as, the storage volume of every EV is 19 kWh [32]. The needed energy for the journey has been defined to be 40% of the maximum volume, that means the EV is entered the parking area with the SOC of 40%. Figure 5 has been depicted the minimum SOC, and time-of-use (TOU) requirements of the EV users. It must be noted that the SOC of EVs is not allowed to be zero and the zero value of SOC, shown in Figure 5 indicates that the corresponding EV is not available in the parking lot.

The data of the DU, the water system, and its demand are derived from [33]. It is assumed that a DU generates 1 L of fresh water by consuming 2.5 kW of electrical power. Three cases are designed in Table 2 to demonstrate the effectiveness of the suggested layout. As can be seen in this table, different type of technologies such as ESS, MT, FC, HP, and etc., as well as regenerative braking energy, and network reconfiguration is considered in case study I. In case study II, the regenerative braking energy, and different type of technologies is considered. But in case study III, the regenerative breaking energy is not considered, and only the network reconfiguration, with different type of technologies is investigated. The specifications of

TABLE 4 Normalized output power of DERs, market and metro prices and AC-MG load factor.

Hour	Market-price ($/kWh)	Metro-price ($/kWh)	Load factor (AC MG)	WT (p.u output power)	PV (p.u output power)	Thermal energy demand (p.u)
1	0.23	0.36	0.6	0.119	0	0.22
2	0.19	0.36	0.65	0.119	0	0.13
3	0.14	0.36	0.59	0.119	0	0.14
4	0.12	0.36	0.62	0.119	0	0.14
5	0.12	0.36	0.7	0.119	0	0.15
6	0.2	3	0.698	0.061	0	0.18
7	0.2	0.36	0.71	0.119	0	0.24
8	0.2	0.36	0.79	0.087	0.08	0.45
9	1.5	2	0.86	0.119	0.15	0.6
10	4	2	0.9	0.206	0.301	0.7
11	4	3.3	0.98	0.585	0.418	0.6
12	4	3.3	1	0.694	0.478	0.52
13	1.5	3.3	0.99	0.261	0.956	0.51
14	4	3.3	1	0.158	0.842	0.49
15	2	3.3	0.97	0.119	0.315	0.48
16	1.95	3.3	0.958	0.087	0.169	0.5
17	0.6	2	0.935	0.119	0.022	0.55
18	0.41	2	0.86	0.119	0	0.58
19	0.35	2	0.88	0.0868	0	0.56
20	0.63	2	0.91	0.119	0	0.53
21	1.17	2	0.927	0.0868	0	0.51
22	0.64	2	0.887	0.0868	0	0.5
23	0.3	2	0.78	0.061	0	0.47
24	0.26	2	0.7	0.041	0	0.38

TABLE 5 Costs in test cases.

No. of cases	Total operation cost ($)	Power loss cost ($)
Case I	62636.77	3200.44
Case II	67473.13	8036.81
Case III	68088.75	3051.03

the utilized trail system are provided in Table 3. Additionally, Table 4 shows the normalized output power of the DERs and market and metro prices along with the AC-MG and thermal load factor.

4.2 | Discussion

Table 5 shows the operation cost and the imposed cost on the operator because of the power losses corresponding to each case. As revealed by Table 5, the lowest operation cost is related to Case I. These results indicate the key role of the regenerative braking energy technology and the network reconfiguration on the total system cost. Moreover, Table 5 indicates that the entire power loss of Case II is higher than Case I. The simulation results illustrate that the power loss cost of Case I is diminished by around 60.18% in comparison with that of Case II. This shows the high impact of the network reconfiguration on the total power loss. In addition, Table 5 shows the vital role of the metro regenerative braking energy in reducing the total system cost because of transferring the braking energy to the metro and the EV parking stations. As revealed by Table 5, the operation cost of Case I is diminished by about 8.00% in comparison with that of Case III. In the following, the results of case studies are discussed.

4.2.1 | Case studies I and II

Table 6 displays the optimal output power of the MTs, the ESS, the FC, the HP, the AC–DC converter, and the DU as well as the transferred braking energy from the metro to the EV parking stations, the purchased power from the upstream grid, the available energy of EV parking stations, and the volume of the primary tank for Case I. Moreover, the network reconfiguration results are presented in the second column of Table 6. The sec-

TABLE 6 Optimal scheduling of the SC in Case I and Case II.

Hour	Opened switches	MT 1 (kW)	MT 2 (kW)	ESS (kW)	FC (kW)	HP (kW)	AC–DC converter (kW)	DU (kW)	Metro to EV parking (kW)	Utility grid (kW)	SOC of EV Parking 1 (kWh)	SOC of EV parking 2 (kW)	Volume of primary tank (L)
1	7,14,8,17,24	0	0	−340	0	119	362	83	0	4345	1446	0	13
2	7,13,9,32,24	0	0	−350	0	70	369	75	0	2805	1474	0	23
3	7,12,10,32,24	0	0	−324	0	76	344	79	0	2578	1511	0	35
4	6,13,9,31,24	0	0	−345	0	75	367	53	0	2666	1535	0	36
5	6,14,9,32,24	0	0	−343	0	82	369	98	0	3208	1714	0	55
6	6,12,9,32,24	0	0	−330	0	98	371	111	0	3635	1143	0	65
7	6,13,10,32,24	4	17	−350	68	131	318	112	0	4254	570	608	75
8	7,13,21,32,24	0	0	−350	0	246	401	114	0	5061	285	1307	94
9	6,12,8,17,24	350	2000	350	700	324	−1384	88	0	1032	0	1605	94
10	6,14,8,16,24	350	2000	350	700	378	−1431	59	0	634	0	1724	80
11	6,14,8,15,24	332	1982	323	693	326	−1500	62	90	490	0	1889	61
12	7,14,10,17,24	300	1732	287	664	279	−1447	27	0	440	0	1884	31
13	6,13,10,17,24	305	1996	312	698	284	−1500	122	6	576	0	1900	20
14	7,14,11,16,24	342	2000	346	677	264	−1500	72	0	603	0	1752	1
15	6,14,8,17,24	350	2000	348	700	259	−1415	105	0	940	0	1747	1
16	6,12,8,16,24	340	2000	342	700	274	−1357	78	0	911	0	1748	2
17	6,14,21,30,24	228	609	344	700	300	−1221	65	31	2728	791	950	3
18	7,13,10,30,24	15	1	−290	650	318	−316	56	0	3884	1197	703	1
19	6,13,9,31,24	0	25	−291	420	304	−60	60	31	4346	1779	399	7
20	6,14,10,30,24	350	515	311	650	288	−1253	69	0	2265	1874	0	15
21	6,14,8,16,24	350	2000	300	700	278	−1344	19	0	733	1879	0	0
22	6,14,10,15,24	350	807	0	700	275	−1003	49	0	2045	1868	0	0
23	6,14,11,31,24	7	0	−38	83	254	−3	50	1	3263	1883	0	0
24	7,14,10,31,24	0	6	−350	9	207	396	25	0	3307	1882	0	0

TABLE 7 Optimal scheduling of the SC in Case III.

Hour	Opened switches	MT 1 (kW)	MT 2 (kW)	ESS (kW)	FC (kW)	HP (kW)	AC–DC converter (kW)	DU (kW)	Metro to EV parking (kW)	Utility grid (kW)	SOC of EV Parking 1 (kWh)	SOC of EV parking 2 (kW)	Volume of the primary tank (L)
1	7,12,10,31,24	0	0	−350	0	119	372	162	0	3949	840	0	45
2	6,12,9,32,24	0	0	−350	0	70	369	51	0	2729	933	0	45
3	7,12,9,32,24	0	0	−344	0	76	363	99	0	2945	1321	0	65
4	6,14,11,31,24	0	0	−342	0	77	365	26	0	2721	1551	0	55
5	6,14,10,31,24	0	0	−350	0	80	375	12	0	2917	1732	0	40
6	6,13,9,31,24	0	0	−344	0	98	374	113	0	3685	1140	0	50
7	6,13,9,30,24	0	0	−350	0	132	390	134	0	4072	570	228	69
8	7,14,11,32,24	0	0	−338	0	245	390	78	0	5071	285	929	72
9	6,13,8,16,24	350	1827	280	686	327	−1300	87	0	986	0	1087	72
10	7,13,8,16,24	76	1964	332	684	384	−1124	28	0	659	0	956	43
11	6,14,9,16,24	338	1892	345	666	327	−1500	17	0	29	0	871	5
12	6,14,9,16,24	350	1750	247	679	285	−1476	88	0	298	0	875	0
13	6,13,8,17,24	343	2000	273	700	275	−1500	229	0	635	0	1082	34
14	6,13,10,16,24	328	1982	336	700	274	−1500	70	0	488	0	1121	12
15	6,13,8,16,24	350	2000	346	700	268	−1413	132	0	837	0	1221	23
16	6,14,10,16,24	350	2000	350	700	273	−1375	19	0	845	0	1520	0
17	6,13,10,30,24	350	718	278	700	302	−1277	129	0	2289	302	950	27
18	6,13,11,30,24	128	7	−272	652	315	−449	122	0	3841	634	703	51
19	6,14,11,30,24	0	0	−135	277	308	−74	2	0	3977	974	399	34
20	7,13,9,15,24	279	1049	349	700	291	−1270	121	0	1874	1027	0	62
21	6,14,8,17,24	350	2000	350	698	275	−1341	0	0	569	1010	0	40
22	6,14,10,17,24	350	1275	79	700	274	−1144	55	0	1448	1042	0	42
23	6,14,11,31,24	0	0	−312	65	252	−297	15	0	3356	1042	0	28
24	7,13,11,31,24	0	4	−291	0	207	346	2	0	3101	1049	0	19

ond column shows the switches which are opened during the specified hour. According to the assumed market price, the market price for off-peak hours, that is, hours between 1 ∼ 8, peak hours, that is, period 9 ∼ 16, and mid-peak hours, that is, period 17 ∼ 24, is low, high, and medium, respectively. According to Table 6, most of the loads are fed through the upstream grid during the off-peak hours. In addition, the ESS is charged during the off-peak period to reduce the operation cost. As revealed by Table 6, an effort has been made to increase the volume of the primary water tank during the off-peak period. It is noted that the AC sub-grid is injected power to the DC sub-grid during off-peak hours to charge the battery and supply loads in the DC sub-grid by purchasing cheap electricity from the upstream grid. In a nutshell, to reduce the operation cost, an effort has been made to supply loads by the upstream grid within the off-peak hours. Furthermore, it is shown that at the peak hours, when the market price is high, entire DERs have been operated close to their maximum production volume to prevent buying costly power from the upstream network. It is noteworthy that the regenerative braking energy back to the trains happens within high-price hours to diminish the energy cost of the metro.

To show the efficiency of the suggested scheme, it is beneficial to compare the results with similar research works. However, since this paper is the first study considering all mentioned technologies in SC, the results cannot be compared numerically with any other work (because the test case is completely different to prior studies). Nonetheless, in [20], which is similar research, the price has been improved about 53 percent when optimized. Here, the price is improved about 62 percent compared to the base case where no optimal scheduling scheme is utilized. This shows the superiority of the proposed scheme when incorporating smart transportation, and network reconfiguration.

For Case II, the optimum output power of the DERs, the AC–DC converter, the DU, and the regenerative braking energy are the same as in Case I. The only difference here is that none of the switches operate. Hence, there exists no network reconfiguration that causes the difference in the power loss cost according to Table 5.

4.2.2 | Case study III

Table 7 shows the optimal output for Case III. In the third case, where there is no regenerative braking energy from metro to EVs, it can be seen that the bought power from the upstream

network is high during off-peak and mid-peak periods. Additionally, it can be observed that the power purchased is higher than in the previous scenarios. The reason is that the regenerative braking energy that is used to supply the metro system itself along with charging EVs, is not available in this case so the required power for the metro system and EVs must be purchased from the up-stream grid and the DERs. This has caused the entire operation cost of Case III to be higher than the previous ones. Similar to the previous cases, the ESS is being charged within off-peak and mid-peak periods when the electricity prices are low, and being discharged within the peak hours when the power prices are high. Moreover, all of the DERs are operating near their maximum within peak hours to diminish the operation costs.

5 | CONCLUSIONS

The BBO algorithm has been applied to optimize the operation of a SC in this paper. The comprehensive SC model is comprised of a power distribution system, a thermal energy system, a water system, a private transportation system, and a public transportation system. The RUT technique has been applied to take the uncertainties of the problem. The suggested problem is tested on a modified 33-bus trail network. As it is observed from the simulation results, it is illustrated through the three case studies that the regenerative braking energy along with system reconfiguration can lower the operation cost of the comprehensive SC model. Future works may include other uncertainties that is able to be arised and are not considered here. Moreover, other optimization algorithms must be compared with the BBO algorithm that is used here in the complexity, time efficiency, and accuracy aspects. Furthermore, cloud-fog computing will be implemented in this type of large-scale system to reduce the computational burden.

NOMENCLATURE

Parameters and Constants

N	Number of DERs
N^{AC}	Number of DERs in AC sub-grid
N^{DC}	Number of DERs in DC sub-grid
N^{EV}	Number of available individual EVs in a parking lot
K^{AC}	Number of buses in AC sub-grid
K^{DC}	Number of buses in DC sub-grid
T	Number of time steps in a day
H	Number of nodes in the thermal energy network
P^{L}	Power load in kW
P^{Heat}	Heat demand in kW
W^{demand}	Water demand in L
RR	Ramp rate
θ	Line impedance phase
Y	Line admittance magnitude
$\eta^{C,ESS/EV}$	Charging efficiency for EESs/EV parking lots
$\eta^{D,ESS/EV}$	Discharging efficiency for EESs/EV parking lots
$S^{Ind,min}$	Minimum SOC level of an individual EV
BC	Battery capacity of an individual EV in kWh
$P^{Metro\ Act}$	Actual value of the metro consumption power in kW
CF^{DU}	Coefficient of energy consumption of desalination unit (DU) in kW/L
λ	Purchasing/selling tariff of DERs in \$/kW
λ^{G}	Purchasing/selling tariff of upstream grid in \$/kW
λ^{ON}	Startup cost
λ^{OFF}	Shutdown cost
λ^{Heat}	Purchasing tariff of thermal energy network in \$/kW
λ^{Water}	Purchasing tariff of the water system in \$/L
λ^{EV}_{deg}	Degradation cost of EV batteries
Δt	Time step duration

Indices and sets

DER	Set of distributed energy resources (DERs)
DER^{AC}	Group of DERs in the AC sub-grid
DER^{DC}	Adjust of DERs in the DC sub-grid
t	Time step
i	Index of DERs

Functions and variables

u	Binary indicator of DER
P	Power purchased/sold from/to DER in kW
P^{G}	Power purchased/sold from/to the main network in kW
P^{C}	Power that is transferred by the bidirectional converter in kW
$P^{loss,AC}$	Power loss in AC sub-grid in kW
$P^{loss,DC}$	Power loss in DC sub-grid in kW
$P^{inj,AC}_{t}$	Injected active power in AC sub-grid in kW
$Q^{inj,AC}_{t}$	Injected reactive power in AC sub-grid in kW
P^{Line}	Power flow through line in kW
$P^{Metro-EV}$	Transferred power from the metro to the EV parking
$P^{EV-Metro}$	Transferred power from the EV parking to the metro
P^{Termal}	Heat purchased from the thermal energy system in kW
$S^{ESS/EV}$	Stored energy in an EES/EV parking in kWh
$S^{EV,Arr}$	Stored energy in EVs at the arrival time
$S^{EV,Dep}$	Stored energy in EVs at the departure time
U^{PT}	Primary tank volume in m^3
U^{FWT}	Fresh water tank volume in m^3
$W^{DU,in}$	Input water of DU in L
$W^{DU,out}$	Output water of DU in L

W^G	Purchased water from the water grid in L
V	Magnitude of the voltage
δ	Phase of the voltage
$B^{C,ESS/EV}$	Charging binary indicator for ESSs/EV parking lots
$B^{D,ESS/EV}$	Discharging binary indicator for ESSs/EV parking lots
$B^{Metro-EV/EV-Metro}$	Binary indicator for interaction between metro-EV parking/EV parking-metro
P^{Bra}	Amount of the braking power that is backed to the metro system in kW

Symbols and acronyms

min, max Minimum and maximum

Indices and sets

- j Index of DERs with type i
- k Index of buses
- v Index of individual EVs
- h Index of nodes in the thermal energy network

AUTHOR CONTRIBUTIONS

Masoud Shokri: Formal analysis; investigation; resources; software; validation; writing—original draft. **Taher Niknam**: Conceptualization; project administration; supervision; validation; visualization; writing—review and editing. **Mojtaba Mohammadi**: Formal analysis; investigation; resources; software; writing—original draft. **Moslem Dehghani**: Conceptualization; data curation; methodology; resources; validation; visualization; writing—original draft; writing—review and editing. **Pierluigi Siano**: Conceptualization; methodology; resources; supervision; validation; visualization; writing—review and editing. **Khmaies Ouahada**: Conceptualization; methodology; validation; writing—review and editing. **Miad Sarvarizade-Kouhpaye**: Investigation; resources; software; writing—review and editing.

CONFLICT OF INTEREST STATEMENT

The authors declare no conflicts of interest.

DATA AVAILABILITY STATEMENT

Data is contained within the article.

ORCID

Taher Niknam https://orcid.org/0000-0002-9391-6901
Moslem Dehghani https://orcid.org/0000-0002-1214-5974

REFERENCES

1. Winkowska, J., Szpilko, D., Pejić, S.: Smart city concept in the light of the literature review. Eng. Manage. Production Serv.11(2), 70–86 (2019)
2. Kamyab, H., Klemeš, J.J., Van Fan, Y., Lee, C.T.: Transition to sustainable energy system for smart cities and industries. Energy 207, 118104 (2020)
3. Rani, S., Mishra, R.K., Usman, M., Kataria, A., Kumar, P., Bhambri, P., Kumar Mishra, A.: Amalgamation of advanced technologies for sustainable development of smart city environment: A review. IEEE Access 9, 150060–150087 (2021)
4. Abdel-Basset, M., Hawash, H., Chakrabortty, R.K., Ryan, M.: Energy-net: A deep learning approach for smart energy management in IOT-based smart cities. IEEE IoT J. 8(15), 12422–12435 (2021)
5. Duan, Q., Quynh, N.V., Abdullah, H.M., Almalaq, A., Do, T.D., Abdelkader, S.M., Mohamed, M.A.: Optimal scheduling and management of a smart city within the safe framework. IEEE Access 8, 161847–161861 (2020)
6. Yang, H., Shen, W., Yu, Q., Liu, J., Jiang, Y., Ackom, E., Dong, Z.Y.: Coordinated demand response of rail transit load and energy storage system considering driving comfort. CSEE J. Power Energy Syst. 6(4), 749–759 (2020)
7. Parhoudeh, S., Baziar, A., Lopez, P.E., Moazzen, F.: Optimal stochastic energy management of smart city incorporating transportation system and power grid. IEEE Trans. Ind. Appl. (2020)
8. Zhang, L., Cheng, L., Alsokhiry, F., Mohamed, M.A.: A novel stochastic blockchain-based energy management in smart cities using V2S and V2G. IEEE Trans. Intell. Transp. Syst. 24(1), 915–922 (2022)
9. Oikonomou, K., Parvania, M.: Optimal coordinated operation of interdependent power and water distribution systems. IEEE Trans. Smart Grid 11(6), 4784–4794 (2020)
10. Dong, W., Yang, Q.: Data-driven solution for optimal pumping units scheduling of smart water conservancy. IEEE IoT J. 7(3), 1919–1926 (2019)
11. Chen, G., Yan, B., Zhang, H., Zhang, D., Song, Y.: Time-efficient strategic power dispatch for district cooling systems considering evolution of cooling load uncertainties. CSEE J. Power Energy Syst. 8(5), 1457–1467 (2021)
12. Chen, G., Zhang, H., Hui, H., Song, Y.: Fast Wasserstein-distance-based distributionally robust chance-constrained power dispatch for multi-zone HVAC systems. IEEE Trans. Smart Grid 12(5), 4016–4028 (2021)
13. Gallego, L.A., López-Lezama, J.M., Carmona, O.G.: A mixed-integer linear programming model for simultaneous optimal reconfiguration and optimal placement of capacitor banks in distribution networks. IEEE Access 10, 52655–52673 (2022)
14. Mahdavi, M., Alhelou, H.H., Bagheri, A., Djokic, S.Z., Ramos, R.A.: A comprehensive review of metaheuristic methods for the reconfiguration of electric power distribution systems and comparison with a novel approach based on efficient genetic algorithm. IEEE Access 9, 122872–122906 (2021)
15. Azizivahed, A., Arefi, A., Ghavidel, S., Shafie-Khah, M., Li, L., Zhang, J., Catalão, J.P.: Energy management strategy in dynamic distribution network reconfiguration considering renewable energy resources and storage. IEEE Trans. Sustainable Energy 11(2), 662–673 (2019)
16. Qiao, X., Luo, Y., Xiao, J., Li, Y., Jiang, L., Shao, X., Xu, J., Tan, Y., Cao, Y.: Optimal scheduling of distribution network incorporating topology reconfiguration, battery energy system and load response. CSEE J. Power Energy Syst. 8(3), 743–756 (2020)
17. Jafari, M., Kavousi-Fard, A., Niknam, T., Avatefipour, O.: Stochastic synergies of urban transportation system and smart grid in smart cities considering V2G and V2S concepts. Energy 215, 119054 (2021)
18. Sheikh, M., Aghaei, J., Chabok, H., Roustaei, M., Niknam, T., Kavousi-Fard, A., Shafie-Khah, M., Catalão, J.P.: Synergies between transportation systems, energy hub and the grid in smart cities. IEEE Trans. Intell. Transp. Syst. 23(7), 7371–7385 (2021)
19. Kavousi-Fard, A., Niknam, T., Fotuhi-Firuzabad, M.: Stochastic reconfiguration and optimal coordination of V2G plug-in electric vehicles considering correlated wind power generation. IEEE Trans. Sustainable Energy 6(3), 822–830 (2015)
20. Cheng, T., Zhu, X., Gu, X., Yang, F., Mohammadi, M.: Stochastic energy management and scheduling of microgrids in correlated environment: A deep learning-oriented approach. Sustainable Cities Soc. 69, 102856 (2021)
21. Rahbari, O., Vafaeipour, M., Omar, N., Rosen, M.A., Hegazy, O., Timmermans, J.M., Heibati, S., Van Den Bossche, P.: An optimal versatile control approach for plug-in electric vehicles to integrate renewable energy sources and smart grids. Energy 134, 1053–1067 (2017)

22. Aien, M., Fotuhi-Firuzabad, M., Aminifar, F.: Probabilistic load flow in correlated uncertain environment using unscented transformation. IEEE Trans. Power Syst. 27(4), 2233–2241 (2012)
23. Gupta, S., Maulik, A., Das, D., Singh, A.: Coordinated stochastic optimal energy management of grid-connected microgrids considering demand response, plug-in hybrid electric vehicles, and smart transformers. Renewable Sustainable Energy Rev. 155, 111861 (2022)
24. Julier, S.J., Uhlmann, J.K.: Reduced sigma point filters for the propagation of means and covariances through nonlinear transformations. In: Proceedings of the 2002 American Control Conference, pp. 887–892. IEEE, Piscataway, NJ (2002)
25. Simon, D.: Biogeography-based optimization. IEEE Trans. Evol. Comput. 12(6), 702–713 (2008)
26. Bhattacharya, A., Chattopadhyay, P.K.: Biogeography-based optimization for different economic load dispatch problems. IEEE Trans. Power Syst. 25(2), 1064–1077 (2009)
27. Wesche, T.A., Goertler, C.M., Hubert, W.A.: Modified habitat suitability index model for brown trout in southeastern Wyoming. North Am. J. Fish. Manage. 7(2), 232–237 (1987)
28. Rathi, A., Sadda, A., Nebhnani, L., Maheshwari, V.M., Pareek, V.S.: Optimal allocation of distributed static series compensators in power system using biogeography based optimization. In: Proceedings of the2012 IEEE 5th India International Conference on Power Electronics (IICPE), pp. 1–6. IEEE, Piscataway, NJ (2012)
29. Leveringhaus, T., Kluss, L., Bekker, I., Hofmann, L.: Solving combined optimal transmission switching and optimal power flow sequentially as convexificated quadratically constrained quadratic program. Electr. Power Syst. Res. 212, 108534 (2022)
30. Calvillo, C.F., Sánchez-Miralles, Á., Villar, J.: Synergies of electric urban transport systems and distributed energy resources in smart cities. IEEE Trans. Intell. Transp. Syst. 19(8), 2445–2453 (2017)
31. PluginCars. Eight Tips to Extend Battery Life of Your Electric Car. http://goo.gl/ExBCTW (2019). Accessed:
32. Chevrolet Pressroom—United States—Spark EV', media.gm.com. https://media.gm.com/content/media/us/en/chevrolet/vehicles/spark-ev/2016.html. (2019). Accessed:
33. Esapour, K., Moazzen, F., Karimi, M., Dabbaghjamanesh, M., Kavousi-Fard, A.: A novel energy management framework incorporating multi-carrier energy hub for smart city. IET Gener. Transm. Distrib. 17(3), 655–666 (2023)

How to cite this article: Shokri, M., Niknam, T., Mohammadi, M., Dehghani, M., Siano, P., Ouahada, K., Sarvarizade-Kouhpaye, M.: A novel stochastic framework for optimal scheduling of smart cities as an energy hub. IET Gener. Transm. Distrib. 18, 2421–2434 (2024). https://doi.org/10.1049/gtd2.13202